Research Article | Vol. 26, No. 23 | 12 Nov 2018 | OPTICS EXPRESS 30634
Optics EXPRESS

Nanofocusing in SOI-based hybrid plasmonic metal slot waveguides

NICHOLAS A. GÜSKEN, MICHAEL P. NIELSEN, NGOC B. NGUYEN, STEFAN A. MAIER, AND RUPERT. F. OULTON*

The Blackett Laboratory, Imperial College London, London SW7 2AZ, UK
**r.oulton@imperial.ac.uk*

Abstract: Through a process of efficient dielectric to metallic waveguide mode conversion, we calculate a >400-fold field intensity enhancement in a silicon photonics compatible nanofocusing device. A metallic slot waveguide sits on top of the silicon slab waveguide with nanofocusing being achieved by tapering the slot width gradually. We evaluate the conversion between the numerous photonic modes of the planar silicon waveguide slab and the most confined plasmonic mode of a 20 x 50 nm^2 slot in the metallic film. With an efficiency of ~80%, this system enables remarkably effective nanofocusing, although the small amount of inter-mode coupling shows that this structure is not quite adiabatic. In order to couple photonic and plasmonic modes efficiently, in-plane focusing is required, simulated here by curved input grating couplers. The nanofocusing device shows how to efficiently bridge the photonic micro-regime and the plasmonic nano-regime whilst maintaining compatibility with the silicon photonics platform.

1. Introduction

Overcoming the diffraction limit of light using metallic components has opened up the door to focusing light down to the nanoscale. The ability to bridge the gap between the microscopic and the nanoscopic regime is of interest in a variety of potential applications ranging from electro-optic modulators [1–4], optical interconnects and routing [5] to nonlinear optics [6,7] and sensor technology [8–10]. The capability to focus light into metal gaps which are only tens of nanometres wide is in particular valuable for plasmonic electro-optical modulation [11]. Strong field enhancements within metallic nano-gaps also enable addressing quantum emitters [12] and high order non-linear processes [1] whose signatures are typically extremely weak.

In principle, nanofocusing can be remarkably effective by using gradually tapered metallic waveguides, where adiabatic mode conversion along the structure precludes inter-mode conversion [13–15]. However, early works on adiabatic nanofocusing did not consider the complete focusing process starting from length scales, where multiple modes can interfere with the nanofocusing process. Moreover, only a few works deal with the experimental reality of having to couple light from a conventional dielectric waveguide or a diffraction limited beam into a nanofocusing metal structure, and none of these provides adiabatic conversion [5,16–21]. Here we explore the nanofocusing process for a signal composed of multiple modes of a planar silicon on insulator (SOI) slab waveguide coupling into the most confined mode of a metallic slot waveguide. By means of finite difference time domain (FDTD) simulations, we consider the complete process of coupling from a focused free space Gaussian beam into a SOI slab using a curved grating which allows for consecutive inherent focused propagation down a plasmonic metal taper and into a metal slot. We found that ~80% of light coupled to SOI modes is converted to the fundamental plasmonic gap mode, which is remarkably close to the predicted adiabatic limit of 96%, as estimated below.

#342256 https://doi.org/10.1364/OE.26.030634
Journal © 2018 Received 15 Aug 2018; revised 4 Oct 2018; accepted 5 Oct 2018; published 7 Nov 2018

Optics EXPRESS

In order to enable efficient conversion of a signal composed of multiple photonic modes into a single plasmonic mode, both signal-to-mode shape and momentum matching must be considered. A variety of studies [16–19] have approached this challenge by using tapered dielectric waveguides in which the mode energy propagates down to near-nanoscale regime where it eventually couples into a tapered dielectric slot in a metal film, which supports a so-called gap plasmon mode. Although high in-coupling efficiencies have been reported, most of these studies are restricted to thick metal films of >100 nm or wide gaps >80 nm, and are thus not able to access the strongest optical confinement possible. One exception is Ono et al. [19], who achieve in-coupling efficiencies of about 70% for a 20 nm thick metal film and a 50 nm wide gap, using an air cladding (i.e. refractive index n = 1). Here however, we study a cladding index of $n \approx 1.5$ which is more practical with respect to the refractive indices of active cladding materials required for optoelectronic applications. Following our previous studies, we explore an alternative route making use of coupling into a nano-gap via a hybrid plasmonic gap waveguide (HPGW) [20–23]. A schematic of the focusing process is shown in Fig. 1. An externally focused free space beam couples to the modes of an SOI slab waveguide via a grating coupler, which are subsequently nanofocused to the confined plasmonic mode by a gradual tapering of the hybrid gap plasmon waveguide. The most efficient nanofocusing requires a curved in-coupling grating to guarantee the best modal shape matching. Momentum matching is explored through the adiabatic criterion, which ensures a gradual increase in mode momentum as it approaches the plasmonic confined state. This results in >80% in-coupling efficiency from the slab into the gap mode. The structure investigated exhibits a small footprint with metal gaps of 20 nm and smaller enabling a >400-fold peak field intensity enhancement. The system is designed in such a way that the gap can be filled with materials such as polymers featuring refractive indexes ≥1.5 making it valuable for electro-optical modulation and non-linear optics while being fully compatible with the SOI platform.

2. The hybrid plasmonic waveguide system

The system under study is illustrated in Figs. 1(a)–1(c). It consists of a 50 nm thick tapered gold waveguide structure and $h = 25$ nm thick SiO_2 spacer layer on top of a $t = 220\,nm$ thick Si layer with 3 μm buried oxide underneath according to standard SOI wafer dimensions. Curved gratings [24–27] which are etched into the Si serve to couple a transverse electric (TE) free space Gaussian beam into the Si slab while also focusing the generated in-plane modes of the slab to a focal spot whose position is determined by the grating's radius of curvature. The structure then converts light from the predominantly TE polarized photonic slab modes into the TE polarized plasmonic gap mode by mode hybridization. The hybrid plasmonic mode can be understood as a coupled mode, based on the coupling between the photonic slab mode and the plasmonic gap mode [22,23]. The waveguide cross sections in Figs. 1(d)-1(f) show the mode profiles at different positions along the guide. For wider gap widths (> 100nm), the energy dominantly resides in the Si slab. The mode area may be gradually decreased by decreasing the gap width ($\boldsymbol{w}$) as shown in Figs. 1(e) and 1(f). For narrow gaps $(w < 100\,nm)$, the energy is eventually confined in the predominantly plasmonic gap mode, as depicted in Figs. 1(d) and 1(g), which provides a strong field intensity enhancement. Interestingly the intensity in the gap shown in Fig. 1(g) does not peak at the very gap start but at about –0.6 μm, after which it decays exponentially due to metal losses.

Optics EXPRESS

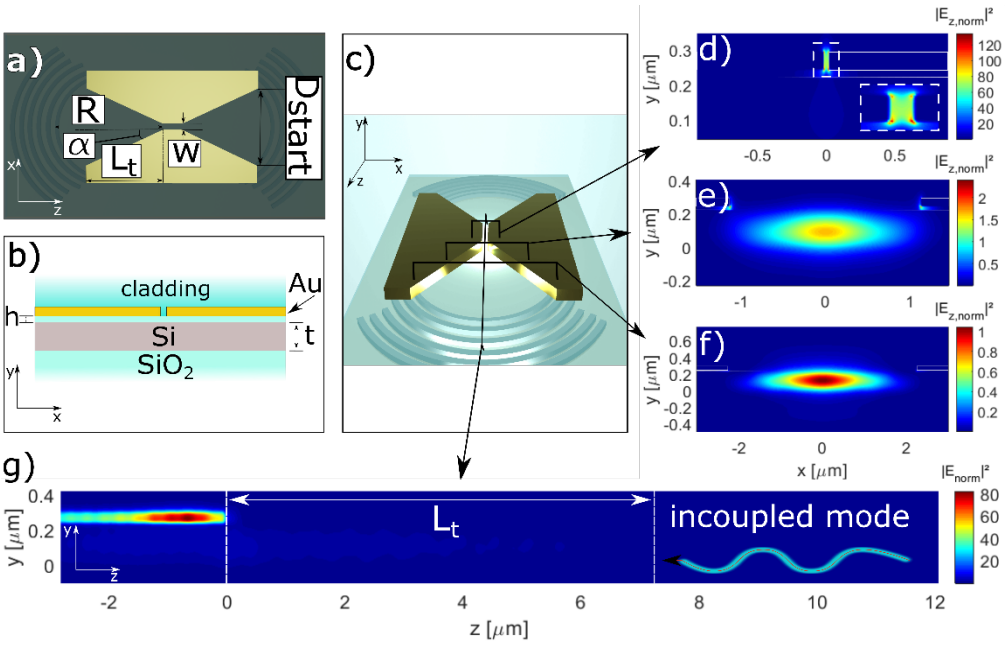

Fig. 1. (a) Topview of the hybrid structure indicating the main parameters: gap width *w*, taper length L_t, taper angle α, grating radius *R* and taper opening D_{start}. (b) Sideview of the structure illustrating the material stack used with t = 220 nm, h = 25 nm, and Au height = 50 nm. The cladding index is n = 1.47 mimicking PMMA [28] and the gratings are placed below the SiO_2 i.e. in the Si slab. The indices used are: $n_{SiO_2} = 1.44$ for SiO_2, $n_{Au} = 0.53 + i \cdot 10.81$ for Au and $n_{Si} = 3.48$ for Si. The gratings are etched into the Si and covered by SiO_2. (c) Sketch of the hybrid taper structure including gratings under illumination. The cross sections at the positions indicated (black rectangles) show the normalized field intensity (equivalent to FE as specified below) profiles in (d)-(f) for taper widths of 4 µm, 2 µm and 40 nm, respectively. The white lines are guidance for the eyes and indicate the metal and upper Si boundaries. The inset in (d) at the lower right shows a close up of the gap region in original scale (Au h = 50 nm, w = 40 nm), highlighted by a white dashed line. (g) Cross sectional sideview along z (through the gap center) showing the field intensity normalized by the intensity in the Si slab only (i.e. without the metal).

The role of the SiO_2 spacer layer in the hybrid system is twofold. Firstly, it contributes significantly to the reduction of plasmonic propagation loss, $\alpha_{loss} \propto \varepsilon_r^{3/2}$, which scales with the real part of the relative permittivity ($\varepsilon_r = \varepsilon_{SiO_2}$) of the metal's cladding [22]. Secondly, the spacer thickness (h) tunes the effective index of propagation, n_{eff}, and defines cut-off conditions for bound modes [23]. Here, a SiO_2 thickness of $h = 25$ nm was chosen to create a strong modal interaction while also assuring compatibility with standard fabrication techniques.

The parameters defining the circular gratings illustrated in Figs. 1 (a) and 1(c) were obtained from 2D FDTD simulations, by optimizing the in-coupling of the TE mode at a wavelength of 1550 nm and using a slightly tilted source angle of 13.45°. Here, a duty cycle $dc = 0.66$ defined as the ratio between the length of the non-etched and etched region in one period along the grating, a pitch $p = 0.66\ \mu m$ defined as the distance from the start of one groove one to the start of the consecutive groove and an etch depth of 100 nm into 220 nm Si are used. A groove radius of curvature, $R = 10\ \mu m$ was chosen (cf. Figure 1 (a)), which also defines the distance from the first grating groove to the start of the gap. The individual grating groove radii are then given by $r_{inner} = R + p(n - dc)$ and $r_{outer} = R + pn$, where $n \in [0,1,2,...]$ is the groove number relative to the inner-most groove.

Optics EXPRESS

The curvature of the gratings enables focusing of a free space beam down to a theoretical mode width $> \lambda / 2n_{eff} = 272\,nm$ in the Si slab, which is within the single mode regime of the hybrid plasmonic waveguide. In the single mode regime, higher order unbound modes may exist but only a single bound mode. However, in practice the full numerical aperture of the curved grating cannot be used, which is why we obtain a minimum mode width of about 1 μm, equivalent to an in-plane numerical aperture of >0.28. The focusing of the mode via curved gratings into the sub 1 μm regime minimizes scattering into unbound and higher order modes of the structure and enables efficient nanofocusing. When using flat in-coupling gratings rather than curved gratings, as in previous demonstrations [20], in-coupling efficiencies around 25% are possible. A one-to-one comparison simulation using flat instead of curved gratings for the structure parameters and beam diameter studied here, shows that the in-coupling efficiency is limited to about 20%. It is useful to point out that the curved grating approximates the time-reversed wavefront of in-plane diffracted waves emitted from the gap plasmon mode [25,29], i.e. an hypothetical wave launched in the gap, diffracted by the slit and propagating towards the grating. Since the wave field is described by the time invariant homogenous wave equation, excellent mode matching can be achieved by imitating the time-inverted wave profile [30].

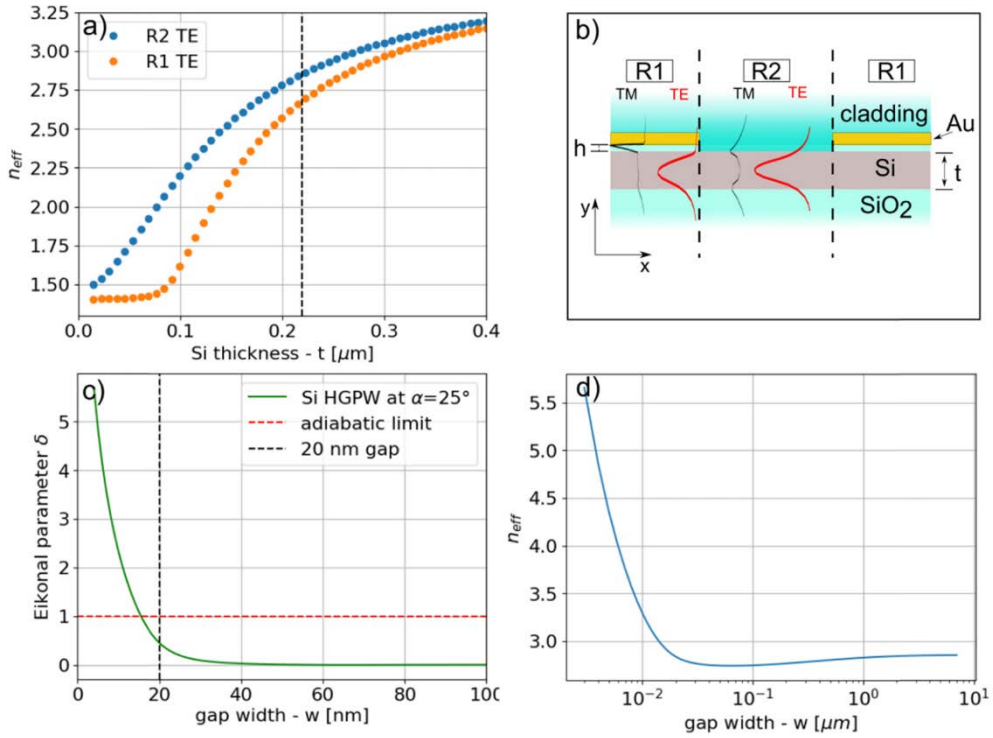

Fig. 2. (a) Calculated n_{eff} in dependence on Si slab thickness (the dashed line indicates the thickness of the HGPW studied) for TE polarization and the regions indicated in (b), calculated via a 2D mode solver using Comsol . (b) Schematics of the the metal loaded region one (R1) and non-metal loaded region two (R2) and its respective position in the structure, superimposed by the according 2D mode solutions in TE and TM polarization. (c), (d) The behavior of the Eikonal parameter (δ) and n_{eff} for a taper angle of α = 25°, respectively, both in dependence on gap width and studied for the fundamental mode.

The hybrid plasmonic waveguide approach exploits metal loading of the underlying SOI waveguide to produce spatial variations in the local effective index (n_{eff}) of in-plane modes, as reported in earlier works [20,23]. In order to find the parameters to maximize in-coupling, we pursued a three-step approach, reducing this complicated 3D problem to lower dimensions.

Optics EXPRESS

Firstly, 1D simulations were performed to evaluate the difference in n_{eff} between metal loaded (R1) and non-metal loaded (R2) regions of the Si slab waveguide. This defined the confinement of modes to the central R2 region and allows us to select the thickness of SiO_2 spacer layer between gold and silicon. For more details on this analysis, we refer to [23]. Secondly, we calculated the n_{eff} of the fundamental mode at each x-y cross section of the taper using a 2D mode solver, shown in Fig. 2 (c) as a plot of n_{eff} vs gap width, *w*. We then used this to evaluate the adiabatic parameter, given in Eq. (1), for the various gap widths, *w*, which allowed us to estimate the maximum taper angle. In this step, we also evaluated the metal loss of the fundamental mode, allowing us to estimate an upper limit for the taper efficiency. Thirdly, we performed full 3D-FDTD simulations to account for Gaussian beam coupling through the curved gratings and to analyze higher order mode conversion throughout the taper. Starting with step one, Figs. 2(a) - (b) compare the modal field distributions of TM and TE modes for the metal loaded SOI (R1) and the SOI-only (R2) regions of the waveguide system, respectively, showing from where the variations in effective index stem. In the case of the TE modes, the metal loaded regions (R1) force the modal field distribution away from the metal, so that it overlaps more with the cladding, thus reducing the effective mode index. This is shown in Fig. 2(a), where the n_{eff} dependence on the Si slab thickness (t) for the two regions (R1 and R2) is plotted for the TE polarization. When patterning metal onto SOI in a R1-R2-R1 configuration (i.e. metal loaded - Si only - metal loaded, cf. Figure 2(b)), TE modes in R2 exhibit the largest n_{eff} enabling energy confinement in the central R2 region. The total n_{eff} of TE-like modes of the structure stays roughly constant at about 2.75 for large gap widths, *w*, eventually increasing rapidly for gap widths $w < 40\,nm$, as shown in Fig. 2(c). This is consistent with strong field confinement for the small gap widths, due to the plasmonic character of the mode.

Following step two, tapering the gap width gradually allows the variation of $n_{eff}(z)$ along the propagation direction, *z*, to be slow enough to prevent back reflections or scattering [14]. The tapering angle was chosen following the Eikonal or adiabatic condition [31]:

$$\delta(z) = \frac{1}{k_0}\left|\frac{d\Re\{n_{eff}(z)^{-1}\}}{dz}\right|, \qquad (1)$$

where k_0 is the wavenumber. The Eikonal parameter, $\delta(z)$, measures how gradual the mode conversion process is at a given position in the taper. For a particular nanostructured taper, there will be a threshold value below which the tapering is gradual enough that mode conversion is considered adiabatic. Based on previous studies we assume that $\delta(z) < 1$, but we will revisit this question later in this work [32]. The taper length and initial gap width were chosen such that $\delta(z = 20\,nm) < 1$ considering gap widths down to $w = 20\,nm$, as shown in Fig. 2(d). The taper length and start width was set to $L_t = 7.5\,\mu m$ and $D_{start} = 7\,\mu m$ which allow a taper angle of about 25°. The third step of our discussion is presented below.

3. Results & discussion: In-coupling efficiency, field enhancement and loss

3D FDTD (Lumerical Solutions) as well as 2D mode-solving (Comsol) simulations were used to study the propagation of light through the taper structure described above at a wavelength of 1.55 μm. A linearly polarized Gaussian beam (~9 μm beam diameter ($1/e^2$) on the grating) illuminates the structure from above and couples TE waves into the SOI waveguide. In order to analyze the propagation behavior of specific modes of interest, the eigenmode-expansion method (EEM) was used to distinguish the individual contributions of each mode to the overall electromagnetic energy propagation. The main results of our study are given in Table 1, which lists the in-coupling efficiency of light from the Si slab into the plasmonic gap mode (η_{inc}) and the electric field intensity enhancement factor (*FE*), which is the ratio between the field

Optics EXPRESS

intensity in the gap and in the slab, all as a function of gap width *w*. The in-coupling efficiency (η_{inc}) is the amount of power transmitted into the fundamental TE mode at the start of the plasmonic gap (cf. Figure 1) divided by the total amount of power coupled into modes of the Si slab by the grating, i.e. $\eta_{inc} = T_{gapstart} / T_{slab.}$ About $T_{slab} \approx 58\%$ of the light is coupled via gratings into the Si-slab and the coupling efficiency from the free space beam into the plasmonic the gap is $\eta_{free} \approx 47\%$ which results in an efficiency from the Si-slab into the gap of $\eta_{inc} \approx 80\%$. The field intensity enhancement factor *FE* is defined as $FE = |E_{gap}|^2 / |E_{slab,0}|^2 = I_{gap} / I_{slab,0}$ where I_{gap} and $I_{slab,0}$ are the peak intensities in the center of the gap and at the start of the Si slab (after the grating), respectively. Experimentally, the field enhancement can be assessed for example via two-photon [13] or three-photon [20] luminescence measurements.

Table 1. In-coupling efficiencies (η_{inc}) and field intensity enhancement factors (*FE*) obtained from 3D FDTD simulations for different configurations defined by the gap width (*w*), the taper opening angle (α) and distance (D_{start}) as well as the taper length (L_t). The strong decrease in in-coupling efficiency for the last configuration is due to the breakdown of the Eikonal approximation for this parameter set, where δ is the Eikonal parameter (cf. Figure 2(c)).

Gap width - *w* [nm]	η_{inc} [%]	*FE*	α [°]	D_{start} [μm]	L_t [μm]	δ
80	79	15	25	7	7.5	≈0.05
60	80	29	25	7	7.5	≈0.07
40	82	86	25	7	7.5	≈0.1
40	72	86	25	2.8	3	≈0.1
20	78	400	25	7	7.5	≈0.5
10	56	1160	25	7	7.5	≈1.7

The results presented in Table 1 show that nanofocusing into gaps down to *w* = 20 nm can be as efficient as $\eta_{inc} \approx 80\%$ while providing a field intensity enhancement >400. The efficiency stays approximately constant for 20 < *w* < 80 nm, while decreasing abruptly to ≈56% for *w* = 10 nm. We attribute this to the increase in scattering and reflection, supported by the fact that the adiabatic parameter increases to $\max\{\delta\} = 1.7$, at 10 nm (cf. Figure 2(c)). Meanwhile, an adiabatic parameter of $\delta(z) < 0.5$, is sufficient to produce effective focusing throughout the taper. The footprint of the system can be reduced, although this comes at a cost of efficiency. Simulations for structures with smaller taper dimensions (L_t = 3 μm, D_{start} = 2.8 μm) show an η_{inc} of 72% for a gap width of 40 nm although maintaining $\delta < 1$. Here, the increase in loss is due to scattering at the narrow taper start (D_{start}) partially impeding the in-coupling of the slab mode into the hybrid system. The FE factors listed in Table 1 increase exponentially with decreasing *w*, highlighting the benefits of efficient coupling to a small gap cross section.

Optics EXPRESS

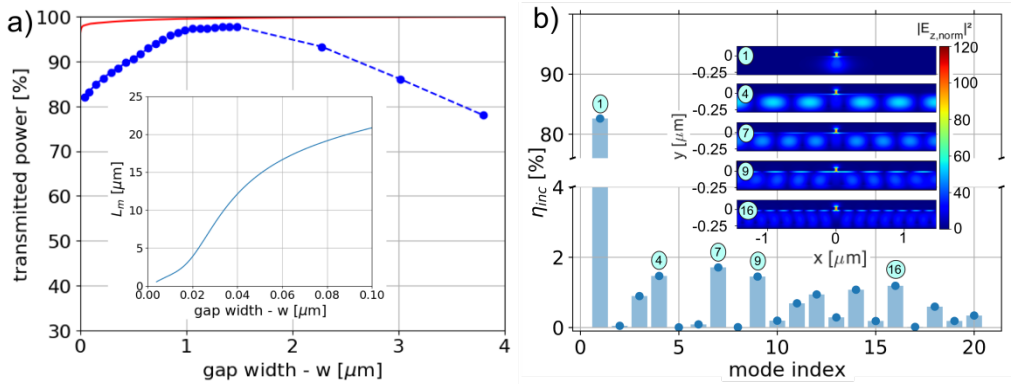

Fig. 3. (a) Power transmitted into the fundamental mode at the waveguide's cross section for different taper widths. The red curve depicts the case of a fundamental mode which is subject to metal losses alone (extracted from 2D mode solving via Comsol). The blue dotted curve shows the actual power loss of the propagating fundamental mode taking all loss channels into account (extracted from 3D FDTD, Lumerical). The inset shows the propagation length L_m vs. taper gap width of the fundamental mode extracted from 2D mode-solver simulations, considering metal losses only. (b) In-coupling efficiency (η_{inc}) into the first 20 modes at the gap start (40 nm gap) obtained from 3D FDTD simulations. The modal cross sections (x-y view) of the five modes into which the main part of the power couples are illustrated on the right according to the respective mode number.

The main contributions to the ≈20% of power lost from the initial signal in the Si (cf. Table 1) during focusing are a) propagation loss (≈4%), b) scattering into other modes (≈11%), c) reflections (≈3%) and d) radiation (<2%). The inset in Fig. 3(a) shows the propagation length L_m of the fundamental mode as a function of the taper width. Long propagation lengths are obtained, exceeding 20 μm for taper gap widths >100 nm which is in line with previous experimental studies [20]. The relation between L_m and the propagation loss, which is mainly due to interaction with the metal is given by $\alpha_{loss} = L_m^{-1}$. The integral over the loss for each position along the entire taper $\int_0^{L_t} \alpha_{loss}(z)\,dz$ gives a total propagation loss of about 4% when tapering down to a 20 nm gap. The total power lost when compared to a waveguide cross section at the beginning and at the end of the taper is estimated via 3D FDTD simulations to be about 7%, which contains metal loss and backscattering. Hence, we estimate that about 3% of the energy is reflected during the tapering.

Figure 3(a) shows the power transmitted into the fundamental mode at different taper positions extracted via the EEM from 3D FDTD simulations (blue dots). The power coupled into the fundamental mode builds up over the taper length while reaching its maximum (around 98%) a gap width between 1 μm - 1.5 μm. The increase in the in-coupled power can be attributed to the inherent focusing providing optimal mode matching closer to the focus. This can be compared to the ideal case in which no power is scattered into other modes estimated via 2D mode solving (red curve, Fig. 3(a)). The comparison shows that scattering into higher order modes is the dominant contribution to losses and occurs in a regime from about $w = 1$ μm down to the beginning of the gap. Figure 3(b) depicts the in-coupling efficiencies into the first 20 modes at the gap start, evaluated via the EEM. Here, all higher order modes are unbound modes as indicated by the mode energy cut off at the simulation boundaries. The various contributions sum up to ≈11% of scattering into higher order modes. We attribute the remaining ≈2% of the total loss to scattering in the vertical direction (radiation loss) which we did not evaluate directly in the simulation.

Optics EXPRESS

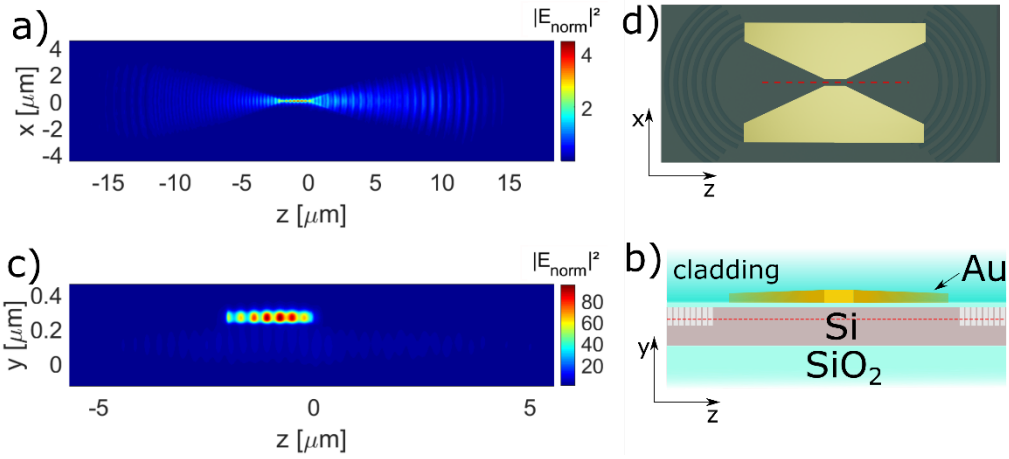

Fig. 4. (a) Horizontal cross section just below the SiO_2 spacer layer depicting the normalized field intensity in the Si taper and below the gap (w = 40 nm). The beam is coupled in from a grating to the right. The curved wavefront is visible in the in- and out-coupling taper regions. (b) Schematic topview of the waveguide structure, the red dotted line indicates the position and length of the crosssection illustrated in (c). (c) vertical cross section along the gap depicting the normalized field intensity of the 40 nm wide gap structure as shown in (a) illustrating the field confinment in the gap only. The structure of the vertical crosssection plotted in (c) is schematicaly shown in (d). The red dotted line indicates the position of the horizontal crosssection plotted in (a).

Figure 4(a) shows the field intensity of the entire structure including in- and out-coupling for a gap width of w = 40 nm and a waveguide length of 2 µm. The power coupled into the slab after the out-coupling taper (propagation from right to the left) was found to be 59% of the initial power in the Si slab, defining the total efficiency of the system. This value can be estimated by taking the 80% in-coupling into the gap and about 16% propagation losses along the 40 nm wide, 2 µm gap into account, leaving 12% of out-coupling loss (scattering and metal losses). Figure 4(b) depicts a cross sectional sideview of the same structure showing strong energy confinement (FE > 80) in the plasmonic gap mode while the energy stays mainly in the Si slab for wider metal width during the in- and out-coupling. The oscillations in the intensity profile observed result from partial backscattering at the end of the gap. The reflection has been estimated via oscillations of the intensity distribution of the field in the gap $I = |a \cdot e^{ikz} + a \cdot r \cdot e^{-ikz}|^2$, where r is the reflection coefficient and a the amplitude. This can be rewritten as $I_{\pm} = a^2(1+r^2) \pm 2a^2 r$, where the normalized intensity profile of Fig. 4 (c) gives the average intensity $a^2(1+r^2) \approx 74$ and the intensity variation $2a^2 r \approx 21$ when taking the peak intensity I_+ = 95 and the adjacent minima I_- = 53 into account. From this, the reflectivity can be estimated to $r^2 \approx 2\%$.

4. Conclusion

We have demonstrated that curved grating in-couplers in conjunction with a hybrid plasmonic nanofocusing approach enable efficient confinement of photonic modes coupled to a SOI platform into narrow (20 x 50 nm^2) metal gaps with an in-coupling efficiency of about 80%. The corresponding electric field intensity enhancement has been determined to be FE > 400. The hybrid structure geometry consisting of a metal taper on a SOI platform was designed in such a way that the adiabatic criterion is fulfilled considering an Eikonal parameter of $\delta < 1$. Although the structure is not fully adiabatic it has been shown that the in-coupling efficiency decreases abruptly if the adiabatic criterion is violated. The hybrid approach allows efficient mode conversion from photonic Si slab to plasmonic gap modes, but the conversion is not adiabatic and the channels of loss have been identified. Here, the main channel of loss can be

Optics EXPRESS

attributed to scattering into higher order modes, which can be reduced by focusing of the slab modes using curved gratings. The total efficiency of the structure, i.e. the total out-coupled power into the bound Si slab modes divided by the injected power at the start of the Si slab has been estimated to ≈59%.

Funding

Leverhulme Trust (RPG-2016-064); Engineering and Physical Sciences Research Council (EPSRC) Reactive Plasmonic Programme Grant (EP/M013812/ 353 1).

Acknowledgment

We acknowledge Guangyuan Li, Alessandro Tuniz, Stefano Palomba and C. Martijn de Sterke from the University of Sydney (NSW, Australia) for initiating discussions on this topic.

References

1. W. Heni, C. Hoessbacher, C. Haffner, Y. Fedoryshyn, B. Baeuerle, A. Josten, D. Hillerkuss, Y. Salamin, R. Bonjour, A. Melikyan, M. Kohl, D. L. Elder, L. R. Dalton, C. Hafner, and J. Leuthold, "High speed plasmonic modulator array enabling dense optical interconnect solutions," Opt. Express **23**(23), 29746–29757 (2015).
2. W. Heni, C. Haffner, B. Baeuerle, Y. Fedoryshyn, A. Josten, D. Hillerkuss, J. Niegemann, A. Melikyan, M. Kohl, D. L. Elder, L. R. Dalton, C. Hafner, and J. Leuthold, "108 Gbit/s Plasmonic Mach-Zehnder Modulator with > 70-GHz Electrical Bandwidth," J. Lightwave Technol. **34**(2), 393–400 (2016).
3. H. W. Lee, G. Papadakis, S. P. Burgos, K. Chander, A. Kriesch, R. Pala, U. Peschel, and H. A. Atwater, "Nanoscale conducting oxide PlasMOStor," Nano Lett. **14**(11), 6463–6468 (2014).
4. C. Hoessbacher, A. Josten, B. Baeuerle, Y. Fedoryshyn, H. Hettrich, Y. Salamin, W. Heni, C. Haffner, C. Kaiser, R. Schmid, D. L. Elder, D. Hillerkuss, M. Möller, L. R. Dalton, and J. Leuthold, "Plasmonic modulator with >170 GHz bandwidth demonstrated at 100 GBd NRZ," Opt. Express **25**(3), 1762–1768 (2017).
5. S. Zhu, T. Y. Liow, G. Q. Lo, and D. L. Kwong, "Silicon-based horizontal nanoplasmonic slot waveguides for on-chip integration," Opt. Express **19**(9), 8888–8902 (2011).
6. W. Cai, A. P. Vasudev, and M. L. Brongersma, "Electrically controlled nonlinear generation of light with plasmonics," Science **333**(6050), 1720–1723 (2011).
7. R. B. Davidson II, A. Yanchenko, J. I. Ziegler, S. M. Avanesyan, B. J. Lawrie, and R. F. Haglund, Jr., "Ultrafast Plasmonic Control of Second Harmonic Generation," ACS Photonics **3**(8), 1477–1481 (2016).
8. S. Naghizadeh, A. Afridi, O. Arisev, A. Karasahin, and S. E. Kocabas, "Experimental Investigation of Stub Resonators Built in Plasmonic Slot Waveguides," IEEE Photonics Technol. Lett. **29**(8), 663–666 (2017).
9. J. N. Anker, W. P. Hall, O. Lyandres, N. C. Shah, J. Zhao, and R. P. Van Duyne, "Biosensing with plasmonic nanosensors," Nat. Mater. **7**(6), 442–453 (2008).
10. J. Jung, T. Søndergaard, and S. I. Bozhevolnyi, "Gap plasmon-polariton nanoresonators: Scattering enhancement and launching of surface plasmon polaritons," Phys. Rev. B Condens. Matter Mater. Phys. **79**(3), 035401 (2009).
11. A. Melikyan, L. Alloatti, A. Muslija, D. Hillerkuss, P. C. Schindler, J. Li, R. Palmer, D. Korn, S. Muehlbrandt, D. Van Thourhout, B. Chen, R. Dinu, M. Sommer, C. Koos, M. Kohl, W. Freude, and J. Leuthold, "High-speed plasmonic phase modulators," Nat. Photonics **8**(3), 229–233 (2014).
12. F. Neubrech, T. Kolb, R. Lovrincic, G. Fahsold, A. Pucci, J. Aizpurua, T. W. Cornelius, M. E. Toimil-Molares, R. Neumann, and S. Karim, "Resonances of individual metal nanowires in the infrared," Appl. Phys. Lett. **89**(25), 1–3 (2006).
13. H. Choo, M. Kim, M. Staffaroni, T. Seok, J. Bokor, S. Cabrini, P. J. Schuck, M. C. Wu, and E. Yablonovitch, "Nanofocusing in a metal-insulator-metal gap plasmon waveguide with a three-dimensional linear taper," Nat. Photonics **6**(12), 838–844 (2012).
14. M. I. Stockman, "Nanofocusing of Optical Energy in Tapered Plasmonic Waveguides," Phys. Rev. Lett. **93**(13), 137404 (2004).
15. C. Ropers, C. C. Neacsu, T. Elsaesser, M. Albrecht, M. B. Raschke, and C. Lienau, "Grating-Coupling of Surface Plasmons onto Metallic Tips: A Nanoconfined Light Source," Nano Lett. **7**(9), 2784–2788 (2007).
16. J. Tian, S. Yu, W. Yan, and M. Qiu, "Broadband high-efficiency surface-plasmon-polariton coupler with silicon-metal interface," Appl. Phys. Lett. **95**(1), 013504 (2009).
17. C.-T. Chen, X. Xu, A. Hosseini, Z. Pan, H. Subbaraman, X. Zhang, and R. T. Chen, "Design of Highly Efficient Hybrid Si-Au Taper for Dielectric Strip Waveguide to Plasmonic Slot Waveguide Mode Converter," J. Lightwave Technol. **33**(2), 535–540 (2015).
18. B. Q. Zhu and H. K. Tsang, "High Coupling Efficiency Silicon Waveguide to Metal–Insulator–Metal Waveguide Mode Converter," J. Lightwave Technol. **34**(10), 2467–2472 (2016).
19. M. Ono, H. Taniyama, H. Xu, M. Tsunekawa, E. Kuramochi, K. Nozaki, and M. Notomi, "Deep-subwavelength plasmonic mode converter with large size reduction for Si-wire waveguide," Optica **3**(9), 999 (2016).
20. M. P. Nielsen, L. Lafone, A. Rakovich, T. P. H. Sidiropoulos, M. Rahmani, S. A. Maier, and R. F. Oulton, "Adiabatic Nanofocusing in Hybrid Gap Plasmon Waveguides on the Silicon-on-Insulator Platform," Nano Lett.

Optics EXPRESS

16(2), 1410–1414 (2016).
21. M. P. Nielsen, X. Shi, P. Dichtl, S. A. Maier, and R. F. Oulton, "Giant nonlinear response at a plasmonic nanofocus drives efficient four-wave mixing," Science **358**(6367), 1179–1181 (2017).
22. R. F. Oulton, V. J. Sorger, D. A. Genov, D. F. P. Pile, and X. Zhang, "A hybrid plasmonic waveguide for subwavelength confinement and long-range propagation," Nat. Photonics **2**(8), 496–500 (2008).
23. L. Lafone, T. P. H. Sidiropoulos, and R. F. Oulton, "Silicon-based metal-loaded plasmonic waveguides for low-loss nanofocusing," Opt. Lett. **39**(15), 4356–4359 (2014).
24. R. Waldhäusl, B. Schnabel, P. Dannberg, E.-B. Kley, A. Bräuer, and W. Karthe, "Efficient Coupling into Polymer Waveguides by Gratings," Appl. Opt. **36**(36), 9383–9390 (1997).
25. Y. Wang, S. Gao, K. Wang, H. Li, and E. Skafidas, "Ultra-broadband, compact, and high-reflectivity circular Bragg grating mirror based on 220 nm silicon-on-insulator platform," Opt. Express **25**(6), 6653–6663 (2017).
26. F. Van Laere, T. Claes, J. Schrauwen, S. Scheerlinck, W. Bogaerts, D. Taillaert, L. O'Faolain, D. Van Thourhout, and R. Baets, "Compact focusing grating couplers for silicon-on-insulator integrated circuits," IEEE Photonics Technol. Lett. **19**(23), 1919–1921 (2007).
27. D. Vermeulen, Y. De Koninck, Y. Li, E. Lambert, W. Bogaerts, R. Baets, and G. Roelkens, "Reflectionless grating couplers for Silicon-on-Insulator photonic integrated circuits," Opt. Express **20**(20), 22278–22283 (2012).
28. F. Languy, K. Fleury, C. Lenaerts, J. Loicq, D. Regaert, T. Thibert, and S. Habraken, "Flat Fresnel doublets made of PMMA and PC: combining low cost production and very high concentration ratio for CPV," Opt. Express **19**, A280–A294 (2011).
29. S. Gao, Y. Wang, K. Wang, and E. Skafidas, "High contrast circular grating reflector on silicon-on-insulator platform," Opt. Lett. **41**(3), 520–523 (2016).
30. G. Leuchs and M. Sondermann, "Time-reversal symmetry in optics," Phys. Scr. **85**(5), 058101 (2012).
31. L. D. Landau and E. M. Lifshitz, *Electrodynamics of Continuous Media* (Pergamon, 1984).
32. D. K. Gramotnev and S. I. Bozhevolnyi, "Nanofocusing of electromagnetic radiation," Nat. Photonics **8**(1), 13–22 (2014).